

Rheological Assessment of a Polymeric Spherical Structure Using a Three-Dimensional Shear Wave Scattering Model in Dynamic Spectroscopy Elastography

Emmanuel Montagnon, Anis Hadj-Henni, Cédric Schmitt, and Guy Cloutier, *Senior Member, IEEE*

Abstract—With the purpose of assessing localized rheological behavior of pathological tissues using ultrasound dynamic elastography, an analytical shear wave scattering model was used in an inverse problem framework. The proposed method was adopted to estimate the complex shear modulus of viscoelastic spheres from 200 to 450 Hz. The inverse problem was formulated and solved in the frequency domain, allowing assessment of the complex viscoelastic shear modulus at discrete frequencies. A representative rheological model of the spherical obstacle was determined by comparing storage and loss modulus behaviors with Kelvin–Voigt, Maxwell, Zener, and Jeffrey models. The proposed inversion method was validated by using an external vibrating source and acoustic radiation force. The estimation of viscoelastic properties of three-dimensional spheres made softer or harder than surrounding tissues did not require *a priori* rheological assumptions. The proposed method is intended to be applied in the context of breast cancer imaging.

I. INTRODUCTION

MECHANICAL properties have been shown to be a reliable indicator of pathological changes in biological tissues [1]. From this finding, modalities using elasticity as an imaging biomarker have been developed in the last two decades and have shown promising clinical results in various areas such as breast cancer or liver fibrosis [2]. In the context of dynamic ultrasound (US) elastography, several inversion methods, such as direct inversion (DI) [3], [4], or shear wave speed measurements from phase shift assessment [5] or time-of-flight in two [6] or three dimensions [7], have been proposed to quantify elasticity. When applied over a frequency range, those latter methods allow estimation of the shear wave speed dispersion (i.e., the frequency dependence of the shear wave speed), and indirectly the viscosity, through the use of a rheological model [5], [8]. However, in cases of confined lesions highlighting a mechanical contrast with the surrounding medium, physi-

cal interactions such as shear wave reflections or scattering affect the robustness of the usual inversion methods, justifying additional processing [9], [10]. In this context, theoretical modeling of shear wave scattering has been proposed to assess the complex shear modulus of confined mechanical heterogeneities [11], [12], or compliance of biological tissues [13]. Such theoretical models have also been successfully applied in the context of a new method called shear wave induced resonance elastography (SWIRE) for viscoelastic characterization of biological tissues [14]–[16].

In the context of breast cancer imaging, lesion shapes and contour irregularities observed at sonography are among the geometrical characteristics assessed in the Breast Imaging Report and Data System classification (BI-RADS) [17], [18]. Lesions with a BI-RADS score of 5 (highly suggesting malignancy) are known to generally exhibit irregular lesion margins (e.g., infiltrated tumors) [19]; however, low-grade categories, including benign lesions, can be approximated by generic geometries [14], [20]. From a mechanical point of view, a strong correlation was found *ex vivo* between tumor elasticity and type I collagen content [21], which is known to exhibit a frequency-dependent shear modulus in the range 0 to 100 Hz [22]. Breast parenchyma has also been demonstrated to be dispersive [23]. Thus, mechanical properties of breast tumors are expected to be frequency dependent, making the measurement of shear storage and loss moduli of confined simple three-dimensional structures over a wide range of frequency clinically relevant [24]. The proposed method is specifically intended to improve the diagnostic specificity of ultrasound for breast cancer imaging.

In this paper, the assessment of the rheological behavior of a 3-D viscoelastic mechanical heterogeneity (inclusion) is demonstrated in the case of a polymeric sphere mimicking a low-grade tumor using a plane shear wave scattering model in an inverse problem approach. The method is validated *in vitro* between 200 and 450 Hz by using an external vibrator linked to a plate (plane waves) and a radiation force source (cylindrical waves). The current paper is organized as follows: the theoretical shear wave scattering model is described, followed by the reference spectroscopy method used for comparison and the inverse problem formulation. To assess the impact of the geometrical assumption and its potential limitations, a robustness evaluation of the proposed inversion method is provided. The third section compares estimated com-

Manuscript received June 26, 2013; accepted November 14, 2013.

The authors are with the Laboratory of Biorheology and Medical Ultrasonics, Université de Montréal Hospital Research Centre (CRCHUM), Montreal, QC, Canada, and the Institute of Biomedical Engineering, Université de Montréal, Montreal, QC, Canada (e-mail: guy.cloutier@umontreal.ca).

A. Hadj-Henni and C. Schmitt are now with Rheolution Inc., Montreal, QC, Canada.

G. Cloutier is also with the Department of Radiology, Radio-Oncology, and Nuclear Medicine, Université de Montréal, Montreal, QC, Canada.

DOI <http://dx.doi.org/10.1109/TUFFC.2014.2908>

plex shear moduli with results of the reference method. The rheological model of the spherical polymeric inclusion is then assessed. Finally, the framework of the proposed elastometry method is extended to radiation force experiments and *in vitro* results are provided. To the authors' knowledge, the proposed method is the first to allow the combination of radiation force excitation with a rheological study on confined 3-D structures.

II. METHODS

A. Theoretical Model

In this section, the theoretical model of plane shear wave scattering by a viscoelastic spherical structure of radius R , embedded in an infinite viscoelastic medium, is presented. The scattering of longitudinal or transverse waves has already been extensively studied in both acoustic and electromagnetic fields [25]. The main modeling steps are presented here; for a detailed presentation, the reader is referred to [26]–[28].

The general equation of motion can be written as

$$(\lambda + 2G)\nabla(\nabla \cdot \mathbf{U}) + G\nabla^2\mathbf{U} = \rho \left(\frac{\partial^2 \mathbf{U}}{\partial t^2} \right), \quad (1)$$

where λ is the first Lamé parameter and G is the complex shear modulus (second Lamé parameter); $G' = \text{Re}(G)$ is the storage modulus and $G'' = \text{Im}(G)$ is the loss modulus; \mathbf{U} is the displacement field; and ρ is the density. Omitting the time-dependent term $\exp(i\omega t)$, the stationary displacement field can be written as the Helmholtz decomposition:

$$\mathbf{U} = Ue^{i\omega t} = \nabla\varphi + \nabla \times \boldsymbol{\psi}. \quad (2)$$

From (1) and (2), two Helmholtz equations, describing longitudinal and transverse displacements are obtained:

$$\nabla^2\varphi_j + k_{Lj}^2\varphi_j = 0 \quad (3)$$

$$\nabla^2\boldsymbol{\psi}_j + k_{Tj}^2\boldsymbol{\psi}_j = 0. \quad (4)$$

In spherical coordinates, solutions of the vector Helmholtz equation, denoted by \mathbf{u} , are expressed using both longitudinal (\mathbf{L}) and transverse terms (\mathbf{M}, \mathbf{N}) in (5). All of those terms are functions of vector spherical harmonics and spherical Bessel or Hankel functions [27].

$$\mathbf{u} = \mathbf{L} + \mathbf{M} + \mathbf{N}, \quad (5)$$

with

$$\begin{aligned} \mathbf{L} &= \nabla\Phi/k \\ \mathbf{M} &= \nabla \times (\mathbf{e}_r r \Psi) \\ \mathbf{N} &= \nabla \times \nabla \times (\mathbf{e}_r r \chi)/k, \end{aligned} \quad (6)$$

and

$$(\nabla^2 + k^2)(\Phi, \Psi, \chi) = 0. \quad (7)$$

As explained in [26], incident (\mathbf{u}_i), scattered (\mathbf{u}_{sc}), and refracted (\mathbf{u}_q) waves can be expressed as

$$\mathbf{u}_i = \sum_n \frac{(2n+1)i^n}{n(n+1)} [\mathbf{M}_{oln}^{(1)}(\mathbf{r}) - i\mathbf{N}_{eln}^{(1)}(\mathbf{r})] \quad (8)$$

$$\mathbf{u}_{sc} = \sum_n \frac{(2n+1)i^n}{n(n+1)} [a_n \mathbf{M}_{oln}^{(3)}(\mathbf{r}) - ib_n \mathbf{N}_{eln}^{(3)}(\mathbf{r}) + d_n \mathbf{L}_{eln}^{(3)}(\mathbf{r})] \quad (9)$$

$$\mathbf{u}_q = \sum_n \frac{(2n+1)i^n}{n(n+1)} [e_n \mathbf{M}_{oln}^{(1)}(\mathbf{r}) - if_n \mathbf{N}_{eln}^{(1)}(\mathbf{r}) + g_n \mathbf{L}_{eln}^{(1)}(\mathbf{r})]. \quad (10)$$

The first subscript of vector functions \mathbf{L} , \mathbf{M} , and \mathbf{N} (o or e) refers to parity; i.e., whether the odd (o, imaginary) or even (e, real) part of the spherical harmonic azimuthal function is used. The second (l) and third (n) subscripts indicate the azimuthal function index and the order of the radial function, respectively. Because the incident wave is purely transverse (9), it does not depend on the longitudinal term \mathbf{L} . Furthermore, scattered waves [outgoing waves indicated by superscript (3)] are expressed in terms of spherical Hankel functions, whereas refracted [superscript (1)] waves are expressed using spherical Bessel functions, which are regular at the origin. In (9) and (10), scattering coefficients $\{a_n, b_n, d_n, e_n, f_n, g_n\}$ are finally computed by specifying elastic boundary conditions at the inclusion boundary ($r = R$); the continuity of both displacements \mathbf{u} and stress $\boldsymbol{\sigma}$ components can be written as

$$\begin{aligned} u_{\zeta i} + u_{\zeta sc} &= u_{\zeta q} \\ \sigma_{r\zeta i} + \sigma_{r\zeta sc} &= \sigma_{r\zeta q} \\ \zeta &= \{r, \phi, \varphi\}. \end{aligned} \quad (11)$$

Once scattering coefficients are known, displacements related to both reflected and scattered waves can be computed at any point of the 3-D space.

B. Polymer Gel Made of Polyvinyl Chloride (PVC) Plastisol

Two polymeric spheres were prepared using a plastic basis solution (lot #2228 LP, M-F Manufacturing Co., Fort Worth, TX) and a plastic softener (lot #4228S, M-F Manufacturing Co.) with respective volume basis/softener ratios of 70%/30% and 85%/15%. The sphere containing the greater softener concentration is hereafter referred to as the soft inclusion; the other is denoted the hard inclusion. To ensure good US backscatter signals, cellulose (Sigmacell cellulose type 50, Sigma Chemical, St. Louis, MO) was added to the solution (0.3 g/20 mL of plastisol solution). Once mixed, the solution was heated to 180°C

and poured into a 7.5-mm-radius spherical mold. Three samples were simultaneously prepared from each mixture for subsequent viscoelastic characterization. After cooling, the spherical inclusion was placed into one liter of agar-gelatin (product numbers G-1890 and A-9799, respectively, Sigma Chemical) to produce experimental phantoms, with respective agar-gelatin weight concentrations of 2% to 3% in water for the hard sphere inclusion phantom, and 3% to 4% for the softer inclusion case. Different concentrations of agar-gelatin were used for both phantoms to assure mechanical contrasts with plastisol inclusions.

C. Reference Spectroscopy Rheometry Method

Reference measurements of PVC plastisol viscoelastic properties were realized using a dynamic rheometer (Rheospectris C-400, Rheolution Inc., Montreal, QC, Canada), allowing rheological studies over a wide range of frequency (from typically 10 to 5000 Hz, depending on materials) [29]. Reference values of complex shear moduli were defined as the mean of three rheometry measures.

D. Experimental Setup

Excitation signals consisted in transient waveforms, generated by the echograph computer (Sonix RP scanner, Ultrasonix Medical Corporation, Burnaby, BC, Canada), and sent to a function generator (33250A, Agilent Technologies Inc., Palo Alto, CA), amplified (type 2706 low-frequency amplifier, Brüel & Kjær, Nærum, Denmark) before supplying a vibrator (type 4810, Brüel & Kjær) mechanically linked to a 150×100 mm plate embedded in a phantom, as illustrated in Fig. 1. An ultrasonic probe (model L14-5/38, 38 mm width, 128 elements, 10 MHz central frequency, Ultrasonix Medical Corporation) was used to acquire RF lines sampled at 40 MHz with 16 bits depth. The ultrasonic beam axis crossed the equatorial plane of the spherical inclusion. To avoid wave reflections at the phantom boundary, an acoustic absorber was embedded within the agar-gelatin gel opposite the US probe. To obtain a frame rate suitable for tracking shear waves, RF-data were collected by pairs of consecutive elements of the probe. For a given data transfer bandwidth, receiving from only two elements with an image depth of 8 cm leads to an increased frame rate compared with standard receiving apertures (typically 32 or 64 elements). The whole probe width was eventually covered by repeating the mechanical excitation 64 times while shifting synchronously active elements [30]. The mechanical excitation was produced with 32 active elements with a 4-cm depth of focus (f-number = 4), and ultrasound data collection was triggered by the scanner computer. This method allowed a frame rate of 3850 Hz to be retrospectively achieved [12], [15]. Such sampling frequency satisfies the Nyquist condition because the considered excitation frequencies did not exceed 500 Hz. Displacements were then estimated by applying a 1-D normalized cross-correlation algorithm on RF data [31]. From temporal transient displacements, the

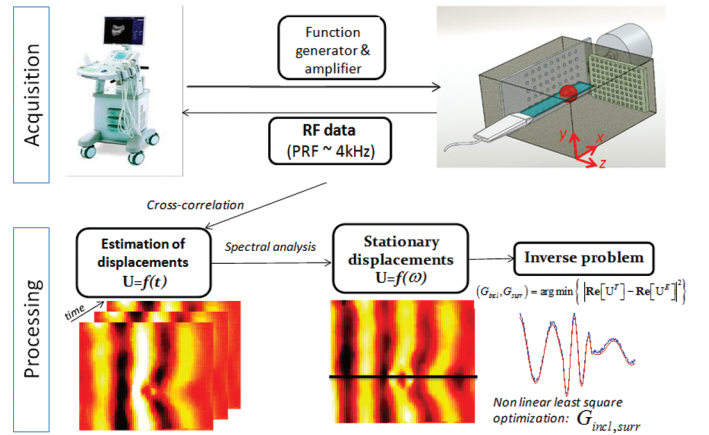


Fig. 1. Experimental data acquisition and post processing. Transient waveforms were converted to mechanical shear waves using a vibrator linked to a plate. RF lines were acquired at an ultrafast frame rate (4 kHz) and processed to estimate induced displacements. From the Fourier transform of displacements, stationary displacement maps were computed over a given frequency range around the excitation frequency. Displacement profiles extracted at multiple frequencies allowed estimation of the frequency dependence of the spherical inclusions' viscoelastic properties.

complex amplitude for each pixel was computed over a typical range of 100 Hz centered on the excitation frequency using a temporal fast Fourier transform (FFT) leading to complex stationary displacement maps [32]. Thus, transient excitation signals allowed investigating larger bandwidths than harmonic signals in a single acquisition [12]. Two series of acquisitions were performed using transient excitations at 245 and 340 Hz central frequency. Excitation waveforms were 6-period-long cosine functions weighted by a Blackman window. This allowed establishment of stationary maps from 200 to 450 Hz without significant loss in SNR.

E. Inverse Problem Formulation

Assuming that the sphere radius and location are known, the theoretical model described earlier could be used to formulate an iterative inverse problem in the frequency domain, based on a nonlinear least squares optimization. The cost function to minimize was formulated as the distance between the real part of displacement fields, where U^T is the theoretical stationary displacement and U^E is the experimental one (see the horizontal black line on the stationary displacement map of Fig. 1, for the case of an inversion considering a single line crossing the center of the inclusion; see details below):

$$(G_{\text{incl}}, G_{\text{surr}}) = \arg \min \left\{ \left| \text{Re}[U^T] - \text{Re}[U^E] \right|^2 \right\} \quad (12)$$

where G_{incl} and G_{surr} are the complex shear moduli of the inclusion and surrounding medium, respectively. Because stationary displacements are complex, the phase must be adjusted between the theoretical and experimental data before distance calculations. A null phase at the first point

of profiles was arbitrarily chosen in the inversion process. The influence of the phase on the inversion accuracy is addressed in the robustness study presented later. Shear storage and loss moduli of the surrounding medium and inclusion were simultaneously estimated in the inversion process for the sake of generality, but also to avoid any potential bias induced by *a priori* fixed surrounding medium viscoelastic parameters. For all inversion occurrences, initial storage moduli were fixed to 10 kPa and loss moduli were set to 0.1ω (which corresponds to a viscosity $\eta = 0.1 \text{ Pa}\cdot\text{s}^{-1}$ in the case of a Kelvin–Voigt model). It is important to note that in this formulation, initial parameters describe a mechanically homogenous medium. Furthermore, no *a priori* assumption is made about the rheological model, as in [32], because the optimized parameters are G' and G'' instead of the elasticity μ and viscosity η .

F. Robustness Study of the Proposed Inversion Method

As previously stated, the estimation of mechanical properties using the proposed inverse problem requires *a priori* known geometrical parameters such as the sphere radius and location, to define the spherical system of coordinates at the origin. In this section, the robustness of the formulated inverse problem is addressed and determined by computing errors on inclusion shear modulus estimation resulting from biased input parameters. First, geometrical biases ranging from -20% to 20% of inclusion properties were successively applied to the sphere radius and position along the three dimensions. Second, as specified in Section II-E, because the stationary displacement profile phase has been arbitrarily chosen at the origin, the impact of such assumption was addressed by considering initial phases ranging from $-\pi/2$ to $\pi/2$, $\pi/8$ angle stepwise. Additionally, to simulate experimental conditions, the influence of the SNR of displacement maps on the inversion process was also investigated by applying zero-mean random noises to reference data from null noise conditions to 8 dB SNR. For each SNR, the inversion was performed ten times to assess mean errors and related standard deviations. Finally, the relevance of the 3-D spherical formulation was evaluated by comparing estimated viscoelastic parameters obtained by using, instead, a model considering 2-D cylindrical geometries [15] in the optimization process. For robustness tests, errors related to an estimated parameter X were computed as

$$\text{Err}(\%) = \frac{X_{\text{estimated}} - X_{\text{reference}}}{X_{\text{reference}}}. \quad (13)$$

For all of the aforementioned conditions, the optimization was performed by considering two distinct input data. The first one, displayed in Fig. 1, considered only one 3.8-cm-width displacement profile, crossing the inclusion center and aligned with the z -axis (shear wave propagation direction), whereas the second was based on eleven 3.8-cm profiles parallel to the z -axis and regularly spaced, from -50% to 50% of the inclusion radius. The goal of

such strategy was to assess whether the estimation accuracy is related to the complex diffraction pattern of the stationary displacement map. In this robustness study, the mechanical inclusion (referred as *incl*) was a theoretical 5-mm-radius sphere exhibiting a complex shear modulus $G_{\text{incl}} = G'_{\text{incl}} + iG''_{\text{incl}}$ of $20 + 3i$ kPa, embedded in a surrounding medium $G_{\text{surr}} = G'_{\text{surr}} + iG''_{\text{surr}} = 5 + 0.25i$ kPa. The excitation frequency in those simulations was chosen at 300 Hz. Such spatio-mechanical configurations are consistent with *in vivo* measurements [23].

G. Rheological Model Assessment

As a complementary assessment of tested materials, the frequency-dependent complex shear modulus of PVC plastisol was matched to different rheological models. Four models were considered [32], [33]: Kelvin–Voigt

$$G_{\text{KV}} = \mu + i\omega\eta, \quad (14)$$

Maxwell

$$G_{\text{M}} = \frac{i\omega\eta\mu}{\mu + i\omega\eta}, \quad (15)$$

Zener

$$G_{\text{Z}} = \frac{\mu_1\mu_2 + i\omega\eta(\mu_1 + \mu_2)}{\mu_2 + i\omega\eta}, \quad (16)$$

and Jeffrey

$$G_{\text{J}} = -\omega\eta_1 \frac{\omega\eta_2 - i\mu}{\mu + i\omega(\eta_1 + \eta_2)}. \quad (17)$$

For both reference (Rheospectris C-400) and experimental US results, (μ_i, η_i) with $i = 1, 2$ being the number of elasticity (μ) and viscosity (η) parameters of each model were estimated by fitting each equation to the complex shear modulus amplitude over the studied frequency range.

H. Acoustic Radiation Force Setup

Experiments using acoustic radiation force as a remote shear wave source were realized using a Verasonics-V1 scanner (Verasonics Inc., Redmond, WA) equipped with an L7-4 probe (Philips Healthcare, Andover, MA). To encounter plane wave conditions in the imaging plane, excitation sequences derived from [34] were used (Fig. 2). Three acoustic bursts (190 μs , 30 V peak-to-peak at 5 MHz) vertically aligned and regularly spaced by a distance $D_2 = 4.6$ mm were generated at $D_3 = 12$ mm laterally to the inclusion center. The second acoustic push of the sequence was horizontally aligned with the inclusion center, which was at $D_1 = 3.5$ cm deep. Adjusting the time delay between consecutive bursts allowed generation of a supersonic cone characterized by a Mach number close to 4 in the surrounding medium [34]. Imaging sequences

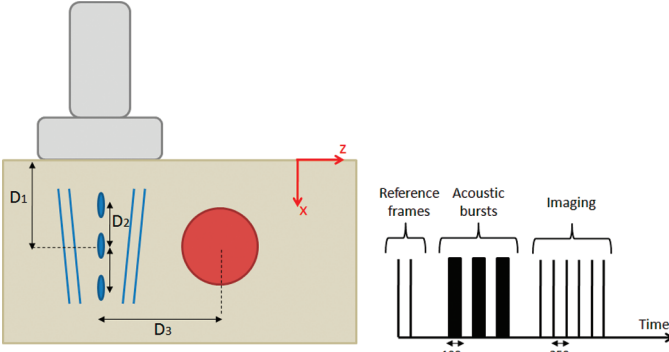


Fig. 2. (a) Acoustic radiation force experimental setup. Three push locations (blue ellipses) separated by $D_2 = 4.6$ mm at $D_1 = 3.5$ cm depth from the probe were generated at a distance $D_3 = 12$ mm from the inclusion's center. (b) Chronology of both acoustic bursts and imaging sequences.

were 100 frames acquired at a frame rate of 4 kHz. Before excitation, reference frames were acquired for subsequent cross-correlation processing. Supersonic shear imaging (SSI) experiments were conducted with the hard plastisol sphere inclusion previously described in Section II-B.

Because of the cylindrical symmetry exhibited by the radiation source geometry (which can be assumed as a line source), displacement amplitudes decreased proportionally to the inverse of the distance to the source in the far field region [35], [36]. Therefore, the observed displacement attenuation was a combination of both geometric scattering and viscous effects related to the propagating medium loss modulus. It has been demonstrated that in the case of a line source, induced displacements can be approximated by [5], [8]

$$u(r) \approx \frac{i}{4} \sqrt{\frac{2}{\pi kr}} \exp(ikr + \pi/4). \quad (18)$$

In (18), without loss of generality, terms in $\exp(i\omega t)$ have been omitted because we consider the general case of a harmonic excitation for this theoretical development. Because $k = \omega/c = 2\pi f/c$, with f the frequency, (18) can be rewritten as

$$u(r) \approx \frac{i}{4\pi} c^{1/2} \sqrt{\frac{1}{fr}} \exp(ikr + \pi/4). \quad (19)$$

Eq. (19) describes a plane shear wave for which amplitude depends on the distance from the source. At a given frequency, the shear wave speed c is constant; therefore, because displacement profiles are normalized in amplitude in the proposed inverse problem formulation, $u(r)$ does not depend on the shear wave speed. To take geometric scattering into account in the inversion process, a weighting term defined as $\sqrt{1/(fr)}$ has been applied to the theoretical modeled data, leading to the following cost function:

$$(G_{\text{incl}}, G_{\text{surr}}) = \arg \min \left\{ \left| \sqrt{\frac{1}{fr}} \mathbf{Re}[U^T] - \mathbf{Re}[U^E] \right|^2 \right\}, \quad (20)$$

where r is the distance to the radiation source location. Considered displacement profiles are horizontal whereas the push axis is vertical; thus in (20), r linearly increases along the z -axis. To determine whether the radial dependence of incident shear wave amplitudes is of interest, both cost function formulations [(12) and (20)] were applied to radiation force experimental data.

III. RESULTS

A. Inverse Problem

Examples of displacement profiles obtained after optimization convergence in the case of hard and soft inclusions are presented in Fig. 3. Inserting estimated solution parameters into the theoretical model (i.e., solving the forward problem) allowed computation of the 2-D displacement maps presented in Fig. 4 (right column). Estimated viscoelastic parameters for both inclusions are compared with results obtained with the reference rheometer between 200 Hz and 450 Hz in Fig. 5. Using (13) at each frequency, mean absolute errors \pm one standard deviations related to estimated G' and G'' over that bandwidth are, respectively, $5.0 \pm 4.8\%$ and $31.6 \pm 18.9\%$ for the hard inclusion, and $6.1 \pm 2.4\%$ and $19.3 \pm 11.6\%$ for the soft case. The inversion process led to surrounding medium elasticity and viscosity of 7.56 ± 0.18 kPa and 0.34 ± 0.13 Pa·s for the hard inclusion case, and 21.2 ± 0.80 kPa and 0.93 ± 0.32 Pa·s for the soft case. Those values were computed from $(G'_{\text{surr}}, G''_{\text{surr}})$ estimated with (12) along the same frequency range and assuming that agar-gelatin mixtures were governed by a Voigt model [37].

B. Robustness Study

1) *Effects of Variance in A Priori Input Geometrical Parameters and of the Number of Displacement Profiles Included in the Inverse Problem:* Complex shear modulus estimation errors for the hard inclusion (i.e., the one presenting the largest variability in Fig. 5) related to biased x, y, z spatial location and radius in the formulation of the inverse problem are presented in Fig. 6. The storage modulus appears robust to biased spatial locations along the three axes, exhibiting errors lower than 10% for all configurations. However, for biased inclusion dimensions, a 26% overestimation of the storage modulus is observed when a 20% underestimation of the inclusion radius was imposed. Errors on loss modulus estimation do not exceed 25% for biased locations along both x and y axes, whereas accuracy is significantly affected by biases applied to the z -axis location or to the inclusion radius. The inversion based on multiple displacement profiles (i.e., eleven instead of one) does not provide improvement in terms of storage modulus quantification. Although slightly better for extreme biases, no noticeable benefit of one formulation compared with the other is also noticed for loss moduli.

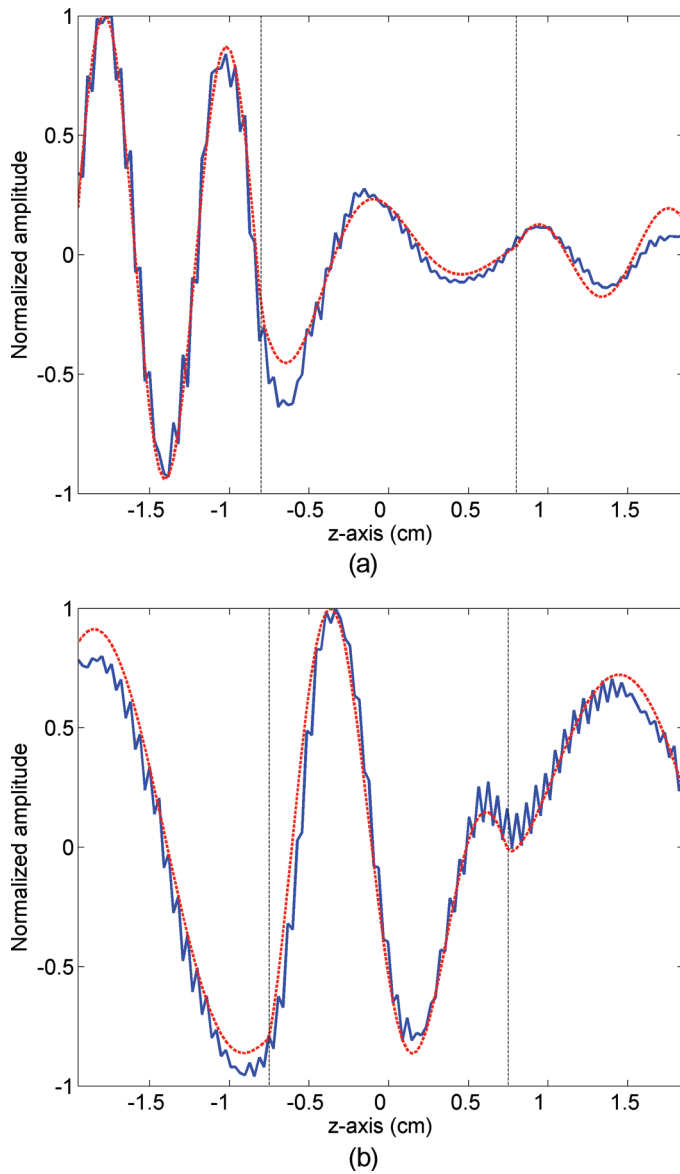



Fig. 3. Experimental displacement profiles (solid blue lines) and theoretical profiles (dashed red lines) obtained by inserting viscoelastic parameters estimated using (12) in the theoretical model (forward problem) for the (a) hard inclusion at 340 Hz and (b) soft inclusion at 245 Hz. Shear waves were mechanically induced by a plate embedded in the phantom. 

2) *Effect of the Initial Phase of the Displacement Profile:* Errors on viscoelastic parameter estimations obtained for various initial phases in the range $[-\pi/2; \pi/2]$ were below 1% for both storage and loss moduli when considering either single or multiple displacement profile formulation. The accuracy of the proposed inversion method thus appears to have little dependence on that parameter.

3) *Effect of the Displacement Profile SNR:* The accuracy of viscoelastic parameter estimations for various SNR conditions is depicted in Fig. 7. For both inversions, considering one or eleven displacement lines, the storage modulus is little affected by the SNR, whereas errors on loss modulus estimations increase as the SNR decreases-

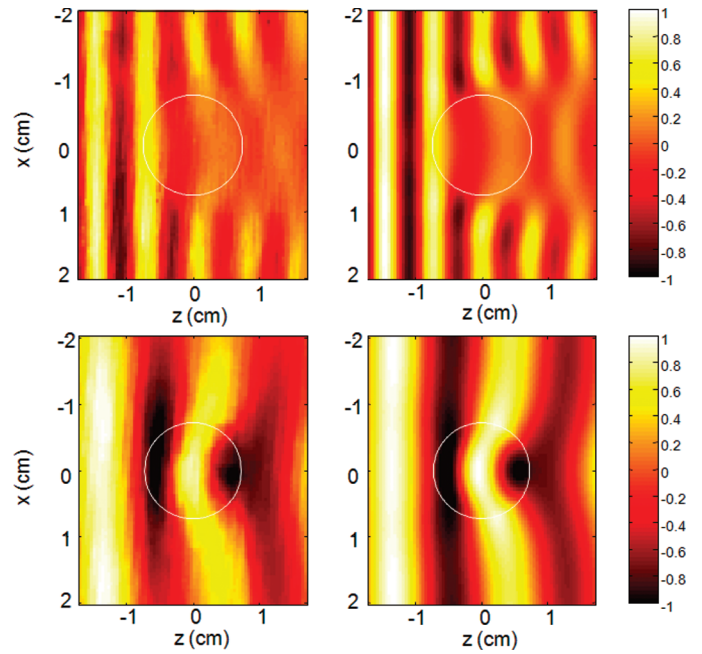



Fig. 4. Displacement maps obtained from experiments (left column) and theoretical ones computed using estimated viscoelastic parameters (right column) for the hard (top row) and soft (bottom row) inclusions. Normalized rms errors between experiments and theory over the whole field of views are, respectively, 9.36% and 7.22%. 

es. Regarding the storage modulus, single and multiple displacement profiles for the inversion perform similarly. However, as the SNR decreases, the loss modulus estimation appears to be less variable when using multiple profiles (standard deviations typically below 10% compared with the case of a single profile for which the standard deviation reaches 38%).

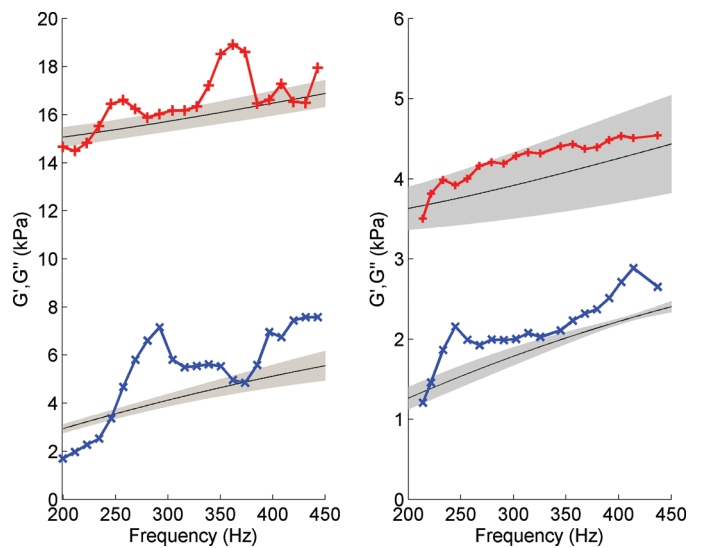



Fig. 5. Storage (top red lines) and loss (bottom blue lines) moduli of the (a) hard and (b) soft spherical inclusions estimated from 200 Hz to 450 Hz. Gray areas indicate standard deviations around mean values (solid black lines) of storage and loss moduli measured using the reference method. 

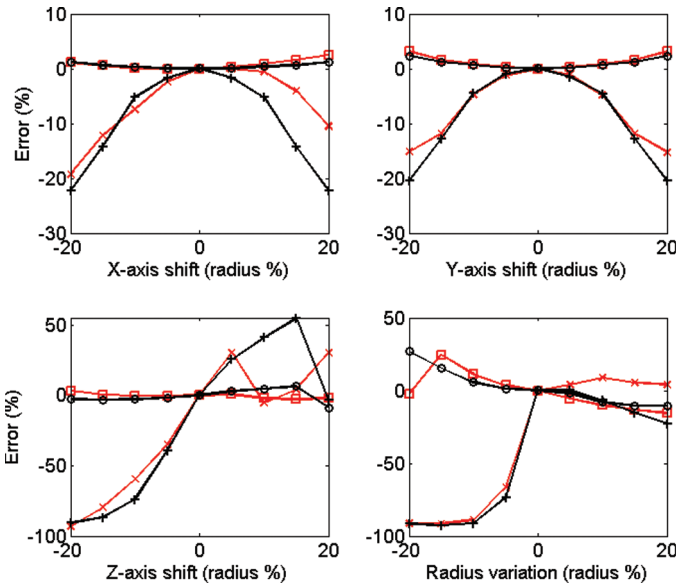


Fig. 6. Errors on viscoelastic estimates obtained for biased input geometric parameters. Black lines indicate the single profile formulation of the inverse problem (circle and plus markers refer to storage and loss modulus errors, respectively), whereas red lines correspond to the multiple profiles formulation (square and \times markers refer to storage and loss modulus errors, respectively).

4) *Effect of a Two-Dimensional Formulation of the Inverse Problem Instead of a 3-D Sphere, as Proposed in this Manuscript:* Fig. 8 presents errors on inclusion complex shear moduli obtained by using a scattering model considering 2-D cylindrical geometries in the minimization process. In the case of a centered position of the considered slice (xz -plane), the storage modulus estimation error is below 10% for both single and multiple displacement profile formulations. However, shifting the slice position along the y -axis induces much larger errors, of up to 200% for the multiple profile case. Similarly, the loss modulus estimation exhibits errors ranging from 65% to 100% for all slice positions along the y -axis. Unlike trends observed in Fig. 6 (3-D spherical model), the 2-D inversion using multiple displacement profiles is clearly less accurate than the case of a single profile.

C. Rheological Model Assessment

The Zener rheological model provided the best fit of the frequency-dependent viscoelastic parameters obtained from plate experiments and the reference rheometry method in the range of 200 to 450 Hz. Related errors on model parameter estimations for both hard and soft plastisol inclusions are indexed in Table I.

D. Acoustic Radiation Force Experiment

From measured radiation-force-induced temporal displacements, the 3-D spherical inverse problem has been applied in the frequency range 200 to 300 Hz, 5 Hz stepwise. The combination of the limited bandwidth of the

mechanical excitation and attenuation with frequency of shear waves in plastisol did not allow investigation of higher frequencies. Mechanical parameters estimated using either (12) or (20) are presented in Fig. 9. Compared with results of the reference rheometry method over the investigated frequency range, mean errors on storage and loss modulus estimations were, respectively, $4.3 \pm 3.0\%$ and $24.1 \pm 14.2\%$ using (20), and $70.5 \pm 18.1\%$ and $274 \pm 29\%$ using (12). The cost function of (20) clearly allowed the best results to be obtained.

IV. DISCUSSION

Using an inverse problem approach, the theoretical model presented in Section II allowed estimation of experimentally complex shear moduli of spherical mechanical inclusions. Estimated viscoelastic parameters were in good agreement with the reference rheometry method over the studied frequency range for plane wave experiments done with both the vibrating plate and the radiation force source. The frequency dependence of complex shear moduli observed in our experiments on PVC plastisol spheres are in agreement with trends highlighted for such material in [29]. However, in the present study, estimations of loss moduli of both hard and soft inclusions exhibited lower accuracy than storage moduli, especially for the hard inclusion case. At a fixed excitation frequency, the main effect of the loss modulus on shear wave propagation was to attenuate displacement amplitudes. Because the shear wavelength is defined as the ratio of the shear wave speed with frequency, low-frequency shear waves propagating in the stiff inclusion led to large wavelengths, complicating

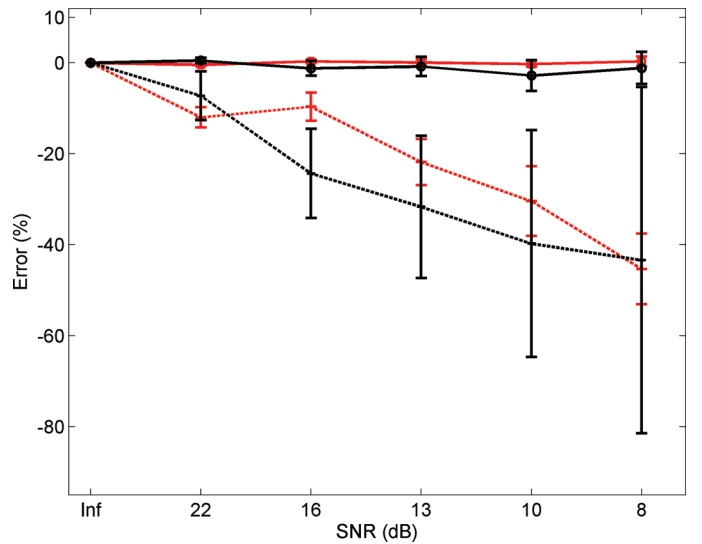


Fig. 7. Effect of displacement profile SNR on viscoelastic parameter estimation accuracy. Red and black lines refer to single and multiple profiles inverse problem formulation, respectively, whereas solid and dashed lines indicate storage and loss modulus estimation errors, respectively. Error bars depict standard deviations obtained after 10 iterations of the inverse problem at each SNR value.

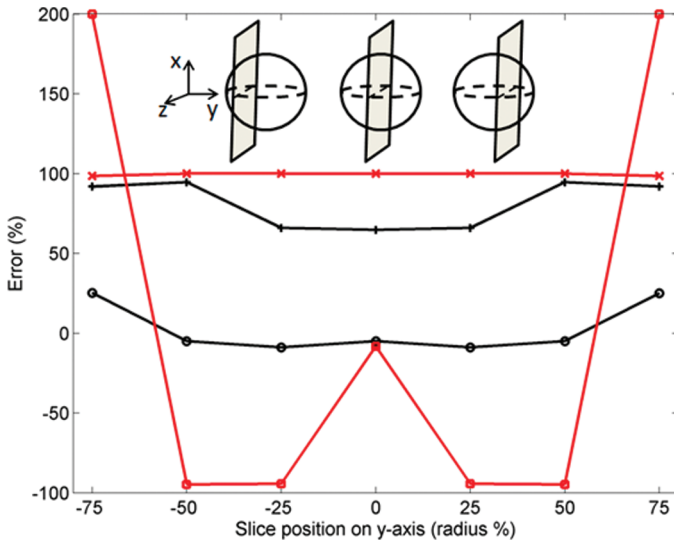


Fig. 8. Errors on spherical inclusion viscoelastic parameter estimation obtained by applying a two-dimensional (cylindrical) theoretical model to displacement profiles for the spherical three-dimensional configuration considering various positions along the y -axis. Black lines correspond to the single profile formulation (circle and plus markers refer to storage and loss modulus errors, respectively), whereas red lines indicate multiple profiles formulation (square and \times markers refer to storage and loss modulus errors, respectively).

the detection of attenuation effect (and of the loss modulus). This point has already been discussed in a previous work [30].

From robustness study results, it was demonstrated that the proposed inversion method is robust to biased inclusion locations along x - and y -axes. In the perspective of future *in vivo* experiments, such robustness to y -axis incorrect positioning is an advantage because this axis corresponds to out-of-plane images. To the contrary, both inclusion size and location along the US propagating axis, and SNR, were major sources of inaccuracy regarding the loss modulus estimation (Figs. 6 and 7). However, because those geometrical parameters can be approximated from B-mode images or elasticity imaging methods [23], those latter are assumed to be measured with reasonable accuracy by taking advantage of existing ultrasound segmentation algorithms [38]. Potential biases arising from sonographic geometry measurements may lead to substantial quantification errors (Fig. 6). This issue could be addressed by performing multiple iterations of the inversion process considering various inclusion radii in the vicinity of the initial measurement. The best solution would then be assessed in terms of distance between theoretical and experimental displacement profiles. Considering Fig. 8, applying an inverse problem formulated using a 2-D shear wave scattering model to 3-D configurations appeared highly inaccurate and sensitive to the inclusion location. Minimum errors were observed at a null slice position along the y -axis. This could be explained because at this position, boundary effects are minimized compared with other positions along the y -axis. Large errors obtained using the 2-D cylindrical model demonstrate the relevance

TABLE I. ZENER PARAMETERS ESTIMATED USING THE INVERSE PROBLEM ON SHEAR WAVE DATA AND FROM DATA OF THE REFERENCE RHEOMETRY METHOD FOR SPHERICAL INCLUSIONS HARDER OR SOFTER THAN THE SURROUNDING MEDIUM.

	Estimated	Rheometer	Error (%)
Hard			
μ_1 (kPa)	13.53	14.50	6.7
μ_2 (kPa)	10.16	11.21	9.4
η (Pa·s ⁻¹)	3.50	2.19	59.8
Soft			
μ_1 (kPa)	3.90	3.38	15.4
μ_2 (kPa)	6.34	5.17	22.6
η (Pa·s ⁻¹)	0.97	0.99	2.0

of the proposed method to estimate viscoelastic properties of spherical inclusions.

To combine the proposed inversion method with an acoustic radiation force excitation, a new cost function to be minimized was formulated to take into account geometrical characteristics of the source. This allowed critical improvements in estimation accuracy (Fig. 9) compared with the standard formulation (12). Indeed, neglecting geometric scattering led to large overestimations of the loss modulus, whereas the storage modulus was underestimated and highly variable. Therefore, the radial dependence of radiation-force-induced displacements cannot be neglected and a straightforward application of the plane wave model (12) in this case is not recommended. Proposed modifications of the plane wave formulation could include either expressing cylindrical outgoing waves with radially dependent amplitudes in spherical coordinates

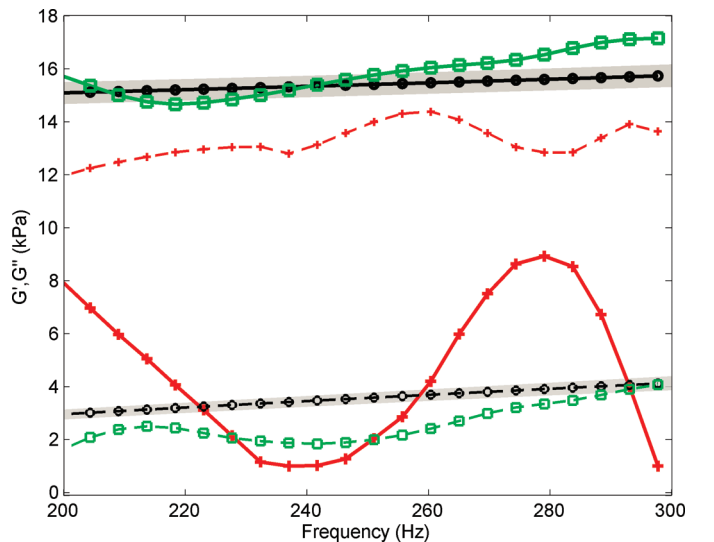


Fig. 9. Experimental storage and loss modulus variations with frequency obtained with the radiation force experiment on the hard inclusion configuration. Black circle markers indicate reference rheometry results, whereas green square and red plus markers represent, respectively, estimations with and without the weighting term in the cost function formulation of (20). For each method, storage and loss moduli are represented by thick full and thin dashed lines, respectively. Gray areas indicate standard deviations around mean values of storage and loss moduli measured using the reference method.

and solving the related linear system of equations (11) or applying the inverse problem to finite element (FE) simulations [20]. Simulations were performed using an eight-core processor (Intel i7-3820; Intel Corp., Santa Clara, CA), clocked at 3.6 GHz, using Matlab software (version 6.5, The MathWorks Inc., Natick, MA). This hardware configuration allowed computation of 128-point displacement profiles (forward problem) similar to those presented in Fig. 3 in 0.310 ± 0.003 s (results from 100 consecutive iterations). Using the FE method, larger computational times are expected, even by taking into account geometrical symmetries of the considered configuration, because the equation of motion (1) must be solved over the whole 3-D volume of interest.

Model-based fitting of complex shear modulus frequency behaviors [$G'(\omega), G''(\omega)$] obtained with both the reference rheometer and experimental measurements (Fig. 5) exhibited minimum errors using the Zener rheological model. For both hard and soft inclusions, the highest bias observed on elasticity parameters of that model was 1.2 kPa (μ_2 , soft inclusion). The viscosity parameter η obtained with the Zener model fitting on shear wave experiments exhibited an error close to 60% in the hard case, whereas it was much better at 2% for the soft inclusion. As observed in Fig. 5, this can be explained by the largest coefficients of variation on G'' in Fig. 5(a), giving higher uncertainties in fitting the frequency-dependent Zener model. Furthermore, whereas fitting experimental data using Maxwell and Jeffrey models led to errors for both elastic and viscous parameters above 50% compared with the reference method, errors on elasticity and viscosity using the Kelvin–Voigt model were respectively 18.3% and 31.0% in the soft case and 8.8% and 59.8% in the hard inclusion situation. For the hard inclusion case, the Kelvin–Voigt model may appear suitable over the investigated frequency range and is simpler than the Zener formulation, because it only requires two parameters. Indeed, the hard inclusion storage modulus exhibited a variation close to 10% from 200 to 450 Hz [Fig. 5(a)], which makes the assumption of a constant value, as in the Kelvin–Voigt model (14), not too restrictive.

Kelvin–Voigt and Maxwell rheological models can be seen as particular cases of Jeffrey and Zener formulations [32], with both requiring fitting of three parameters. Thus, achieving a better fitting using a more complex model seems obvious, but at a cost of a more complex physical interpretation. Considering the Kelvin–Voigt model expression (14), one can see that the storage modulus (real part of G_{KV}) does not depend on frequency, which is not true in the case of the polymeric material used in our experiments (Fig. 5). Thus, assuming the inclusion mechanical properties as governed by a Kelvin–Voigt model would lead to biased elasticity measurements in this case, as previously discussed. Those remarks highlight the importance and potential consequences of the rheological model assumption on the viscoelastic parameter estimation.

The rheological model fitting reliability is tightly influenced by both the robustness of dynamic elastography

measures and by the investigated frequency range (bandwidth). It has been demonstrated experimentally that large frequency ranges can be achieved by radiation force, using amplitude-modulated excitation sequences [39]. Another method takes advantage of acoustic excitation along closed paths to enhance displacements and reduce high-frequency attenuation impact [40]. However, agreement of such strategies with dose limitations required by the US Food and Drug Administration remains to be demonstrated.

As shown in [41], viscoelastic characterization of soft homogeneous media can be achieved through shear wave speed measurements over a large frequency range and the use of an *a priori* known rheological model (the Kelvin–Voigt model is the most commonly used). Shear wave speed can be computed using the following relation:

$$c = \omega \frac{\Delta r}{\Delta \varphi}, \quad (21)$$

where ω is the angular frequency. Δr and $\Delta \varphi$ are the distance and the measured phase difference between two measurement points, respectively. Recently, this method has been successfully applied *in vivo* to study the dispersion phenomenon in the liver [8], as an extension of the SSI method. However, it has been noted that phase gradient methods might be challenged in the case of nonhomogeneous media, e.g., a medium containing a mechanical inclusion, because of the combination of shear wave interactions with the confined structure and increased errors on speed measurements over small propagation distances [5], [41].

As an example corresponding to this latter condition, inserting viscoelastic shear moduli obtained by the reference method for the hard inclusion case in the 3-D theoretical spherical model, and computing the shear wave speed using (21) over the frequency range of 200 to 450 Hz as in reported experiments, led to errors of 39.9%, 17.0%, and 30.6% on μ_1 , μ_2 , and η estimations, respectively. Varying Δr of (21) in our simulations did not provide significant improvements in accuracy. Such results justify modeling of shear wave scattering for viscoelastic characterization of confined mechanical heterogeneities, as studied in this work. We recognize, however, that unlike the phase-gradient or time-of-flight method, the theoretical model and inverse problem formulation require *a priori* knowledge of the sphere radius and location.

Once detected and measured, the proposed inverse problem can retrieve not only the elasticity, but elasticity and viscosity components of the lesion. An important contribution of this work for the *in vivo* applicability of the proposed method was also to prove the feasibility of the inverse problem formulation when acoustic radiation force was considered. As observed by comparing Fig. 9 with Fig. 5(a), similar quantitative results were obtained by using either the vibrating plate (plane wave condition) or a radiation force with a supersonic cone characterized by a Mach number close to 4. By considering geometric scat-

tering [35], [36], radiation pressure experiments coupled to other theoretical scattering models (e.g., cylindrical [12] or elliptical [30] inclusions) are expected to be straightforward because the transition is simply based on applying a dedicated weighting function independently of the geometry considered, as proposed in (21). Note that shear waves propagating in soft tissues might not be exactly plane or cylindrical. In the case of the radiation force experiment, the small propagation distance resulting from geometric scattering (18) allowed us to assume a locally homogeneous medium in the vicinity of the inclusion. Furthermore, slightly distorted wavefronts could be analytically modeled as a summation of shear waves (8) at various phases.

V. CONCLUSION

In this paper, a new method dedicated to the viscoelastic characterization of spherical inclusions in dynamic elastography has been presented and validated *in vitro* using an inverse problem based on a three-dimensional shear wave scattering model. The proposed method has also been extended to the particular case of radiation force experiments, leading to a new formulation of the inverse problem. The proposed method might provide additional information on confined physiological lesions by assessing both storage and loss modulus variations with frequency. Future works may focus on establishing dedicated excitation sequences to achieve a larger bandwidth for optimum rheological model fitting to retrieve the elasticity and viscosity of scanned lesions.

REFERENCES

- [1] J. Ophir, I. Cespedes, and H. Ponnekanti, "Elastography: A method for imaging the elasticity of biological tissues," *Ultrason. Imaging*, vol. 13, no. 2, pp. 111–134, 1991.
- [2] K. J. Parker, M. M. Doyley, and D. J. Rubens, "Imaging the elastic properties of tissue: The 20 year perspective," *Phys. Med. Biol.*, vol. 56, no. 1, pp. R1–R29, 2011.
- [3] S. Catheline, J. L. Gennisson, G. Delon, M. Fink, R. Sinkus, S. Abouelkaram, and J. Culioli, "Measuring of viscoelastic properties of homogeneous soft solid using transient elastography: An inverse problem approach," *J. Acoust. Soc. Am.*, vol. 116, no. 6, pp. 3734–3741, 2004.
- [4] K. Nightingale, M. Palmeri, R. Nightingale, and G. Trahey, "Acoustic remote palpation: Initial *in vivo* results," in *IEEE Ultrasonics Symp.*, 2000, vol. 2, pp. 1553–1558.
- [5] S. Chen, M. Fatemi, and J. F. Greenleaf, "Quantifying elasticity and viscosity from measurement of shear wave speed dispersion," *J. Acoust. Soc. Am.*, vol. 115, no. 6, pp. 2781–2785, 2004.
- [6] M. L. Palmeri, M. H. Wang, J. J. Dahl, K. D. Frinkley, and K. R. Nightingale, "Quantifying hepatic shear modulus *in vivo* using acoustic radiation force," *Ultrasound Med. Biol.*, vol. 34, no. 4, pp. 546–558, 2008.
- [7] S. Lee, J. Chang, W. Kim, M. Bae, N. Cho, A. Yi, H. R. Koo, S. J. Kim, J. Y. Kim, and W. K. Moon, "Differentiation of benign from malignant solid breast masses: Comparison of two-dimensional and three-dimensional shear-wave elastography," *Eur. Radiol.*, vol. 23, no. 4, pp. 1015–1026, 2013.
- [8] T. Defieux, G. Montaldo, M. Tanter, and M. Fink, "Shear wave spectroscopy for *in vivo* quantification of human soft tissues viscoelasticity," *IEEE Trans. Med. Imaging*, vol. 28, no. 3, pp. 313–322, 2009.
- [9] J. Klein, J. McLaughlin, and D. Renzi, "Improving arrival time identification in transient elastography," *Phys. Med. Biol.*, vol. 57, no. 8, pp. 2151–2168, 2012.
- [10] T. Defieux, J. L. Gennisson, J. Bercoff, and M. Tanter, "On the effects of reflected waves in transient shear wave elastography," *IEEE Trans. Ultrason. Ferroelectr. Freq. Control*, vol. 58, no. 10, pp. 2032–2035, 2011.
- [11] E. Montagnon, A. Hadj-Henni, C. Schmitt, and G. Cloutier, "Viscoelastic characterization of an elliptical structure in dynamic elastography imaging using a semi-analytical shear wave scattering model," in *IEEE Ultrasonics Symp.*, 2011, pp. 1163–1166.
- [12] A. Hadj Henni, C. Schmitt, and G. Cloutier, "Three-dimensional transient and harmonic shear-wave scattering by a soft cylinder for dynamic vascular elastography," *J. Acoust. Soc. Am.*, vol. 124, no. 4, pp. 2394–2405, 2008.
- [13] S. Papazoglou, C. Xu, U. Hamhaber, E. Siebert, G. Bohner, R. Klingebiel, J. Braun, and I. Sack, "Scatter-based magnetic resonance elastography," *Phys. Med. Biol.*, vol. 54, no. 7, pp. 2229–2241, 2009.
- [14] A. Hadj Henni, C. Schmitt, I. Trop, and G. Cloutier, "Shear wave induced resonance elastography of spherical masses with polarized torsional waves," *Appl. Phys. Lett.*, vol. 100, no. 13, art. no. 133702, 2012.
- [15] A. Hadj Henni, C. Schmitt, and G. Cloutier, "Shear wave induced resonance elastography of soft heterogeneous media," *J. Biomech.*, vol. 43, no. 8, pp. 1488–1493, 2010.
- [16] C. Schmitt, E. Montagnon, A. Hadj Henni, Q. Shijie, and G. Cloutier, "Shear wave induced resonance elastography of venous thrombi: A proof-of-concept," *IEEE Trans. Med. Imaging*, vol. 32, no. 3, pp. 565–577, 2013.
- [17] E. Lazarus, M. B. Maimiero, B. Schepps, S. L. Koelliker, and L. S. Livingston, "BI-RADS lexicon for US and mammography: Interobserver variability and positive predictive value," *Radiology*, vol. 239, no. 2, pp. 385–391, 2006.
- [18] American College of Radiology, "ACR practice guideline for the performance of breast ultrasound examination," Reston, VA, 2007, pp. 569–573.
- [19] H. Madjar and E. B. Mendelson, Eds. *The Practice of Breast Ultrasound: Techniques, Findings, Differential Diagnosis*. Stuttgart, Germany: Thieme Publishing Group, 2008.
- [20] M. L. Palmeri, S. A. McAleavey, K. L. Fong, G. E. Trahey, and K. R. Nightingale, "Dynamic mechanical response of elastic spherical inclusions to impulsive acoustic radiation force excitation," *IEEE Trans. Ultrason. Ferroelectr. Freq. Control*, vol. 53, no. 11, pp. 2065–2079, 2006.
- [21] S. Barnes, P. Young, and M. Miga, "A novel model-gel-tissue assay analysis for comparing tumor elastic properties to collagen content," *Biomech. Model. Mechanobiol.*, vol. 8, no. 4, pp. 337–343, 2009.
- [22] D. M. Knapp, V. H. Barocas, A. G. Moon, K. Yoo, L. R. Petzold, and R. T. Tranquillo, "Rheology of reconstituted type I collagen gel in confined compression," *J. Rheol.*, vol. 41, no. 5, pp. 971–993, 1997.
- [23] M. Tanter, J. Bercoff, A. Athanasiou, T. Defieux, J.-L. Gennisson, G. Montaldo, M. Muller, A. Tardivon, and M. Fink, "Quantitative assessment of breast lesion viscoelasticity: Initial clinical results using supersonic shear imaging," *Ultrasound Med. Biol.*, vol. 34, no. 9, pp. 1373–1386, 2008.
- [24] E. Lee, H. Jung, K. Ko, J. Lee, and J. Yoon, "Diagnostic performances of shear wave elastography: Which parameter to use in differential diagnosis of solid breast masses?" *Eur. Radiol.*, vol. 23, no. 7, pp. 1803–1811, 2013.
- [25] J. Faran and J. James, "Sound scattering by solid cylinders and spheres," *J. Acoust. Soc. Am.*, vol. 23, no. 4, pp. 405–418, 1951.
- [26] N. G. Einspruch, E. J. Witterholt, and R. Truell, "Scattering of a plane transverse wave by a spherical obstacle in an elastic medium," *J. Appl. Phys.*, vol. 31, no. 5, pp. 806–818, 1960.
- [27] P. M. Morse and H. Feshbach, *Methods of Theoretical Physics*. New York, NY: McGraw-Hill, 1953.
- [28] J.-P. Sessarego, J. Sageloli, R. Guillermin, and H. Uberall, "Scattering by an elastic sphere embedded in an elastic isotropic medium," *J. Acoust. Soc. Am.*, vol. 104, no. 5, pp. 2836–2844, 1998.
- [29] A. Hadj Henni, C. Schmitt, M.-E. Tremblay, M. Hamdine, M.-C. Heuzey, P. Carreau, and G. Cloutier, "Hyper-frequency viscoelastic spectroscopy of biomaterials," *J. Mech. Behav. Biomed. Mater.*, vol. 4, no. 7, pp. 1115–1122, 2011.
- [30] E. Montagnon, A. Hadj-Henni, C. Schmitt, and G. Cloutier, "Viscoelastic characterization of elliptical mechanical heterogeneities using

a semi-analytical shear-wave scattering model for elastometry measures,” *Phys. Med. Biol.*, vol. 58, no. 7, pp. 2325–2348, 2013.

- [31] E. Montagnon, S. Hissouin, P. Despres, and G. Cloutier, “Real-time processing in dynamic ultrasound elastography: A GPU-based implementation using CUDA,” in *11th Int. Conf. Information Science, Signal Processing and their Applications*, 2012, pp. 472–477.
- [32] C. Schmitt, A. Hadj Henni, and G. Cloutier, “Characterization of blood clot viscoelasticity by dynamic ultrasound elastography and modeling of the rheological behavior,” *J. Biomech.*, vol. 44, no. 4, pp. 622–629, 2011.
- [33] D. Klatt, U. Hamhaber, P. Asbach, J. Braun, and I. Sack, “Noninvasive assessment of the rheological behavior of human organs using multifrequency MR elastography: A study of brain and liver viscoelasticity,” *Phys. Med. Biol.*, vol. 52, no. 24, pp. 7281–7294, 2007.
- [34] J. Bercoff, M. Tanter, and M. Fink, “Supersonic shear imaging: A new technique for soft tissue elasticity mapping,” *IEEE Trans. Ultrason. Ferroelectr. Freq. Control*, vol. 51, no. 4, pp. 396–409, 2004.
- [35] S. Calle, J.-P. Remenieras, O. B. Matar, M. E. Hachemi, and F. Patat, “Temporal analysis of tissue displacement induced by a transient ultrasound radiation force,” *J. Acoust. Soc. Am.*, vol. 118, no. 5, pp. 2829–2840, 2005.
- [36] J. Bercoff, M. Tanter, M. Muller, and M. Fink, “The role of viscosity in the impulse diffraction field of elastic waves induced by the acoustic radiation force,” *IEEE Trans. Ultrason. Ferroelectr. Freq. Control*, vol. 51, no. 11, pp. 1523–1536, 2004.
- [37] J. L. Gennisson and G. Cloutier, “Sol-gel transition in agar-gelatin mixtures studied with transient elastography,” *IEEE Trans. Ultrason. Ferroelectr. Freq. Control*, vol. 53, no. 4, pp. 716–723, 2006.
- [38] J. A. Noble and D. Boukerroui, “Ultrasound image segmentation: A survey,” *IEEE Trans. Med. Imaging*, vol. 25, no. 8, pp. 987–1010, 2006.
- [39] M. W. Urban, M. Fatemi, and J. F. Greenleaf, “Modulation of ultrasound to produce multifrequency radiation force,” *J. Acoust. Soc. Am.*, vol. 127, no. 3, pp. 1228–1238, 2010.
- [40] D. Ekeom, A. Hadj-Henni, and G. Cloutier, “Design of a phased array for the generation of adaptive radiation force along a path surrounding a breast lesion for dynamic ultrasound elastography imaging,” *IEEE Trans. Ultrason. Ferroelectr. Freq. Control*, vol. 60, no. 3, pp. 552–561, 2013.
- [41] S. Chen, M. Urban, C. Pislaru, R. Kinnick, Y. Zheng, A. Yao, and J. F. Greenleaf, “Shearwave dispersion ultrasound vibrometry (SDUV) for measuring tissue elasticity and viscosity,” *IEEE Trans. Ultrason. Ferroelectr. Freq. Control*, vol. 56, no. 1, pp. 55–62, 2009.



Emmanuel Montagnon was born in 1982 in Nancy, France. He obtained his B.Sc. degree in theoretical physics from the Université de Nantes and his master’s degree from the Université de Grenoble in 2007. He completed his Ph.D. degree in biomedical engineering in 2013 at the Université de Montreal, where he was conducting his research in the Laboratory of Biorheology and Medical Ultrasonics of the University of Montreal Hospital Research Center. His research interests

include dynamic ultrasound elastography and applications to breast cancer and deep vein thrombosis, shear wave scattering modeling, and plane wave imaging.



Anis Hadj Henni received his degree in civil engineering from the École Polytechnique Nationale d’Algiers in 2002. In 2006, he received his Ph.D. diploma in mechanics from the Université de Bordeaux I for his work on microwave generation of vibrations applied to nondestructive evaluation of structures. In 2006, he joined the Laboratory of Biorheology and Medical Ultrasonics (LBUM, CRCHUM) in Montreal to work on dynamic elastography imaging of soft tissues, as a postdoctoral fellow and then as research associate.

Since 2009, as a result of his research, Dr. Hadj Henni has been the co-founder and President of Rheolution Inc. (www.rheolution.com), a Montreal-based technology company specializing in the development of scientific instruments to characterize the viscoelasticity of soft materials.



Cédric Schmitt was born in 1978 in Hyères, France. He graduated in 2002 from the École Nationale Supérieure des Ingénieurs Électriciens de Grenoble (part of the Institut National Polytechnique de Grenoble), Grenoble, France, majoring in signal processing and systems. In 2003, he joined the Laboratory of Biorheology and Medical Ultrasonics, University of Montreal Hospital Research Center, Montreal, Quebec, Canada, where he received his M.Sc. degree in 2005 and his Ph.D. degree in 2011, both in biomedical engineering from

the Institute of Biomedical Engineering of the University of Montreal. His research was focusing on noninvasive vascular elastography methods for the characterization of atherosclerosis in carotid arteries, and dynamic elastography and micro-elastography techniques for vascular applications. Since 2009, Dr Schmitt has been the co-founder and CTO of Rheolution inc., an innovative company specialized in the design and commercialization of a new generation of mechanical instruments for the viscoelastic measurement of soft materials.



Guy Cloutier (S’89–M’90–SM’07) obtained his B.Eng. degree in electrical engineering from the Université du Québec à Trois-Rivières in 1984, and his M.Sc. and Ph.D. degrees in biomedical engineering from the École Polytechnique de Montréal in 1986 and 1990, respectively. Between 1990 and 1992, he was a postdoctoral fellow at The Pennsylvania State University with Prof. K. Kirk Shung. Prof. Cloutier is Director of the Laboratory of Biorheology and Medical Ultrasonics at the University of Montreal Hospital Research

Center (www.lbum-crchum.com), Professor and Director of Research at the Department of Radiology, Radio-Oncology and Nuclear Medicine of the University of Montreal, and Member of the Institute of Biomedical Engineering at the same Institution. His research interests are in quantitative ultrasound imaging of red blood cell aggregation; quasi-static and dynamic ultrasound elastography of atherosclerotic plaques, vascular aneurysms, deep vein thrombi, and breast cancers; 3-D morphologic and hemodynamic assessment of lower limb arterial stenoses; and mathematical and biomechanical modeling. He has published more than 150 peer reviewed articles in these fields, holds 12 patents, licensed one technology, and was recipient of the National Scientist award of the Fonds de la Recherche en Santé du Québec (2004–2009).